

1.65 μ m (H-band) surface photometry of galaxies. X: Structural and dynamical properties of elliptical galaxies.

Stefano Zibetti¹

Max-Planck-Institut für Astrophysik Karl-Schwarzschild-Str. 1, D-85741 Garching bei München, Germany

zibetti@mpa-garching.mpg.de

and

Giuseppe Gavazzi

Università degli Studi di Milano - Bicocca, P.zza delle Scienze 3, I-20126 Milano, Italy

and

Marco Scodéggiò

Istituto di Fisica Cosmica “G. Occhialini”, CNR, via Bassini 15, I-20133, Milano, Italy

and

Paolo Franzetti¹

Istituto di Fisica Cosmica “G. Occhialini”, CNR, via Bassini 15, I-20133, Milano, Italy

and

Alessandro Boselli

Laboratoire d’Astrophysique de Marseille, BP8, Traverse du Siphon, F-13376 Marseille Cedex 12, France

ABSTRACT

We analyse the structural and dynamical properties of a sample of 324 nearby elliptical and dwarf elliptical galaxies observed during an extensive NIR survey in H-band (1.65 μ m). The Fundamental Plane (FP) is determined and a significant

¹Università degli Studi di Milano - Bicocca, P.zza delle Scienze 3, I-20126 Milano, Italy

tilt is assessed. The origins of such a tilt are investigated by means of a spherically symmetric, isotropic pressure supported dynamical model relying on the observed surface brightness profiles. The systematic variation of the shape coefficient converting the measured central velocity dispersion σ_0 into the virial rms velocity σ_{rms} is found to be the main cause of the tilt, due to aperture effects. Moreover the ratio between the dynamical mass M_{dyn} and the total H-band luminosity L_H turns out to be roughly constant along the luminosity sequence of ellipticals: H-band luminosity is therefore a reliable and cheap estimator of the dynamical mass of the Es.

Subject headings: galaxies: fundamental parameters — galaxies: elliptical and lenticular, cD — galaxies: photometry — infrared: galaxies

1. Introduction

The assumption that normal galaxies are in dynamical equilibrium implies that, for a given type of dynamics (i.e. rotation or pressure supported), the dynamical status of the system is strongly related to its mass distribution. Using the further assumption that the mass inside the “observable” radius of a galaxy is traced by the (stellar) light, the dynamical parameters should be, at least in first approximation, determined by the structural parameters describing the light distribution. In the case of elliptical galaxies, these systems have been proved to be mainly pressure supported and the fundamental dynamical parameter is the central velocity dispersion σ_0 . The simplest way of describing the light distribution of a galaxy is to measure the half light (or effective) radius R_e and the average surface brightness I_e inside R_e . If the elliptical galaxies formed a homologous family, both from the structural and the dynamical point of view, and the M/L ratio were constant, the virial theorem would imply a linear relation between the logarithm of the three parameters given by:

$$\log R_e = 2 \log \sigma_0 - \log I_e + k \quad (1)$$

A linear relation has been actually found (the Fundamental Plane, FP, Djorgovski & Davis 1987; Dressler et al. 1987), but the coefficients differ significantly from those predicted by the virial theorem (this is known as the “tilt” of the FP). This implies the non-constancy of M/L and/or the breaking of the homology. However the existence of the FP as a tight relation requires that the variations of M/L or the breaking of the homology happen in a very systematic way.

Most of the early studies devoted to this problem assumed homology and concluded that a systematic increase of M/L with luminosity is needed both in optical (see e.g. Bender

et al. 1992) and in NIR pass-bands (see e.g. Pahre et al. 1998a). However, many studies, in which the surface brightness profiles are analysed both in optical (see e.g. Djorgovski et al. 1985a,b; Schombert 1986, 1987; Jedrzejewski 1987; de Carvalho & da Costa 1988; Capaccioli et al. 1988) and in NIR pass-bands (see e.g. Gavazzi et al. 2001; Scodéglio et al. 2002), have found systematic variations of the profile shape and concentration index (i.e. the structural parameter quantifying how much the light distribution is centrally peaked²) among ellipticals, implying a breaking of the homology. In pioneering work Prugniel & Simien (1997) and Graham & Colless (1997) produced evidence in favour of a strong influence of structural non-homology on the tilt of the FP. Busarello et al. (1997) concluded that most of the tilt could be accounted for by dynamical non-homology, although spatial non-homology and stellar population effects can give significant contributions as well. More recently, Bertin et al. (2002) showed how the departure from spatial homology contributes to the tilt of the FP in the B band for a small sample of nearby E galaxies imaged with high S/N.

The claim by Scodéglio et al. (1998), that the amount of tilt is significantly lower in the NIR bands than in the optical ones, implies, however, a significant role of different stellar populations (age, metallicity) in determining the M/L and the structural parameters. NIR pass-bands are the most suitable for studying the structural parameters because they trace much better than visible pass-bands the bulk of the luminous mass of the galaxies which sits in old stellar populations. Moreover they are less sensitive to dust obscuration and line blanketing, and in turn this reduces the age/metallicity effects on the M/L ratio. We have performed a systematic and extensive investigation of the structural properties in the H (K') band for a sample of nearby galaxies, covering all the morphological types and extending from high to low luminosities, i.e. to the dwarf regime (see Gavazzi et al. 2000a, 2001, and references therein). Based on these surface brightness profiles, Scodéglio et al. (2002) demonstrate a systematic relationship between the concentration index c_{31} and the total H-band luminosity which is almost completely independent from the eye-ball morphological classification: from this relationship the structural non-homology of the elliptical family can be inferred. The structural and dynamical properties of the whole sample of surveyed galaxies are analysed by Pierini et al. (2002) adopting the κ -space formalism (Bender et al. 1992).

In this paper we present a study of the relationships between the structural H-band ($1.65\mu\text{m}$) properties of 324 elliptical and dwarf elliptical galaxies. The relationships with dynamical parameters are analysed for a subsample of 135 galaxies ranging from the highest luminosities to the dwarf regime and extending the original sample of 73 galaxies studied by Scodéglio

²Many definitions of concentration index were proposed in literature; the definition hereafter adopted is $c_{31} = r_{75}/r_{25}$, the ratio between the radii enclosing 75% and 25% of the total luminosity of the galaxy (see Gavazzi et al. 2001; Scodéglio et al. 2002)

et al. (1998). The sample is described in Sec. 2. In Sec. 3 we study the “Kormendy relation” between the effective surface brightness μ_e and the effective radius R_e . In Sec. 4 a derivation of the H-band FP is presented using different fitting methods, with an analysis of the contribution to the FP tilt due to M/L and homology breaking is performed in Sec. 5, using a simple dynamical model relying on the measured surface brightness profiles. The method, independently developed by Zibetti (2001), is very similar to that of Bertin et al. (2002). It should be stressed, however, that we analysed a 10 times larger sample using NIR photometric data, as opposed to the B band data analysed by Bertin et al. (2002). A brief discussion and the conclusions of this work are given in Sec. 6 and 7.

2. The sample

In this paper we analyse the photometric H-band ($1.65\mu\text{m}$) structural parameters of a sample of 324 “bona fide” elliptical and dwarf elliptical (dE) galaxies selected among members of 5 nearby, rich clusters: namely the Virgo, Coma, A1367, A262 and Cancer clusters, in addition to a significant population of galaxies in the “Great Wall”, the bridge between Coma and A1367. Observations and photometric analysis of this sample are reported by Gavazzi et al. (2000b,a, 2001) (and references therein). The total H-band luminosity L_H , the effective radius R_e (i.e. the radius enclosing half of the total luminosity), the effective surface brightness μ_e , defined as the average surface brightness within R_e , and the concentration index c_{31} are derived from the azimuthally averaged surface photometry (see Gavazzi et al. 2000a). Absolute luminosities and physical radii are calculated attributing to each galaxy the mean cluster (“cloud”) distance, with the exception of the galaxies in the “Great Wall”, for which the redshift distance ($H_0 = 75 \text{ km sec}^{-1} \text{ Mpc}^{-1}$) is assumed.

For a subsample of 135 galaxies dynamical analysis could be performed relying on central velocity dispersion measures (σ_0) obtained from the literature (see Scodéggi et al. 1998, and references therein).

The entire sample comprises: 274 ellipticals (129 with σ_0 measurements) and 50 dwarf ellipticals/spheroidals (6 with σ_0 measurements).

Table 1: Completeness for the Coma Super-cluster and the Virgo cluster

<i>Region</i>	m_{pg}	Log $L_{\text{H}\odot}$	<i>Tot</i>	<i>Photo</i>		<i>Dynamic</i>	
				#	#	%	#
<i>Coma</i>	< 15.7	> 10.5	186	180	(97)	86	(46)
<i>Virgo</i>	< 14	> 9.6	35	31	(89)	25	(71)
	14 ÷ 15	9.6 ÷ 9.1	72	36	(50)	7	(10)
	15 ÷ 16	9.1 ÷ 8.7	99	12	(12)	2	(2)
	16 ÷ 18	8.7 ÷ 7.8	304	6	(2)	0	(0)

Details on the sample completeness in the Coma Super-cluster region ($18^\circ \leq \delta \leq 32^\circ$; $11^h30^m \leq \alpha \leq 13^h30^m$) and the Virgo cluster are given in Tab.1: for each bin of photographic magnitude m_{pg} ($\log L_{\text{H}\odot}$) the total number of galaxies in the CGCG (Zwicky et al. 1968, $m_{\text{pg}} < 15.7$) – for the Coma region – and in the VCC catalogue (Binggeli et al. 1985) – for the Virgo cluster – are given, along with the total number (percentage) of galaxies in the photometric sample and in the dynamical sample. In translating m_{pg} into $\log L_{\text{H}\odot}$ an average colour-luminosity relation of $B - H = 0.3\log L_{\text{H}\odot} + 0.5$ is assumed (see Scudiego et al. 2002). A mean distance modulus of 34.9 is assumed for the Coma region, while a distance of 17 Mpc is attributed to the Virgo A cluster, according to Gavazzi et al. (1999). As far as the photometric parameters are concerned, we cover a representative sample comprising the transition between the giant- and the dwarf-regime. Dynamical measurements are available only for giants, with few exceptions providing some hints on the behaviour of the scaling relations at low luminosity.

3. The Kormendy relation

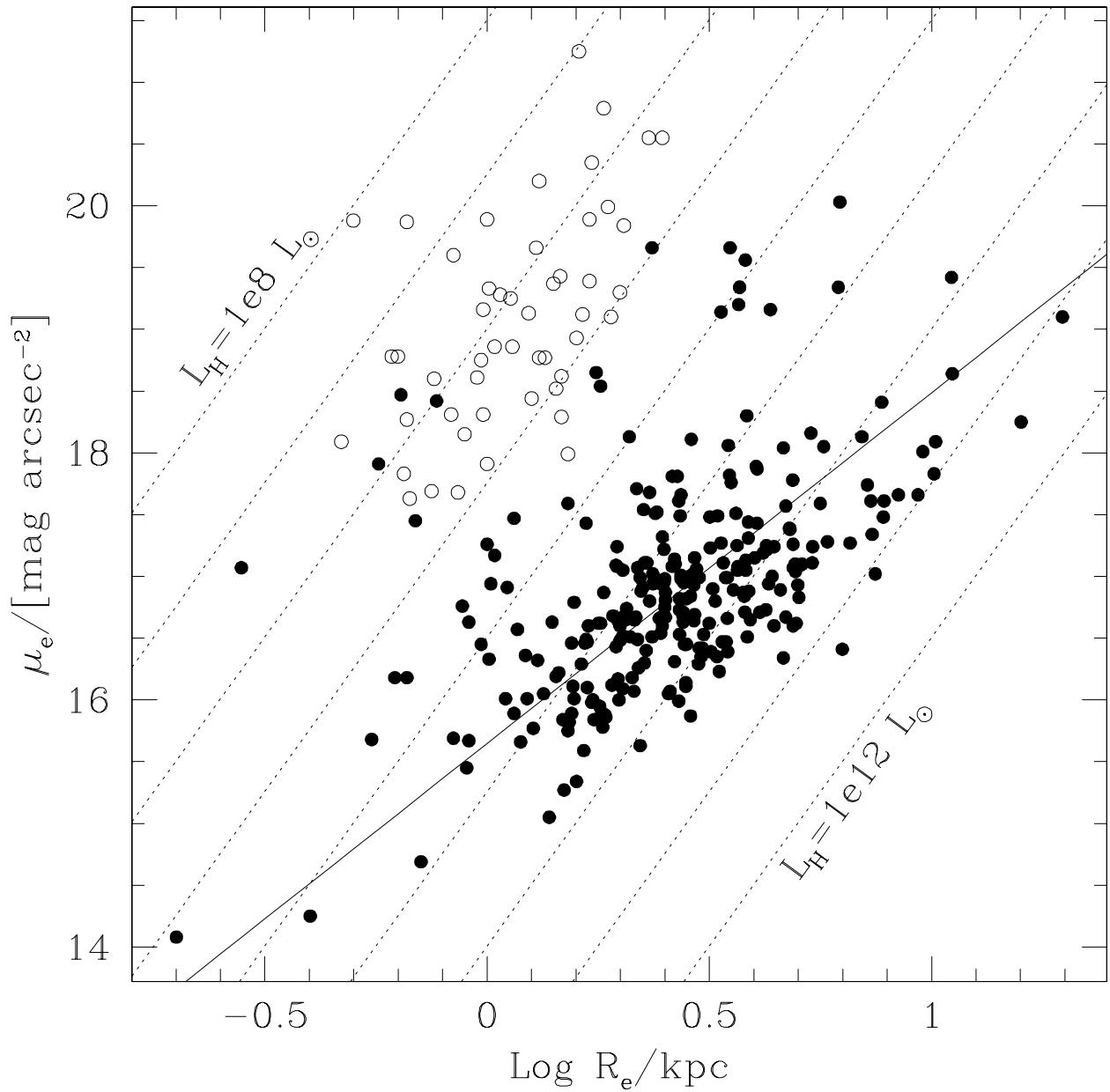


Fig. 1.— The Kormendy relation. Filled symbols are giant ellipticals, empty symbols dwarfs. Iso-luminosity lines are dotted, assuming mean ellipticity 0.35, in 0.5 dex intervals. The continuous line represent the OLSB fit for the giants.

The “Kormendy relation” (Kormendy 1985) between the effective surface brightness μ_e and the effective radius R_e is shown in Fig.1. Filled symbols represent giant ellipticals, empty symbols dwarfs. The dotted lines indicate iso-luminosity loci, assuming a mean ellipticity of 0.35, from 10^8 to $10^{12} L_{H\odot}$. Giant ellipticals follow a mean relation given by $\mu_e = (2.84 \pm 0.06) \cdot \log R_e + (15.65 \pm 0.03)$. This is obtained from an Orthogonal Least Square Bivariate (OLSB) fitting procedure with 3σ rejection, and is represented in Fig.1 by the continuous line. Dispersion is noticeable: 0.62 mag arcsec $^{-2}$. The slope $(-0.88 \pm 0.02$ expressed in $\log (L_{H\odot} \text{ kpc}^{-2})/\log \text{kpc}$) is consistent with -0.83 ± 0.08 as measured by Kormendy & Djorgovski (1989) in the r band.

Low-luminosity and dwarf ellipticals do not follow the same relationship as giants: the latter would imply that galaxies at lower luminosity should be increasingly compact, M32-like objects, while observations show that the lower luminosity of dwarfs is mainly due to their lower surface brightness. However, from Fig.1 no clear dichotomy can be assessed between giants and dwarfs, and it could be argued that, to a first approximation, galaxies populate uniformly the μ_e - R_e space, avoiding the region below the mean Kormendy relation. In other words, for each effective radius there is an upper-limiting effective surface brightness, and this is lower for larger radii.

4. The FP relation

In this section we present a study of the Fundamental Plane relationship between R_e , I_e (defined by $\log I_e/L_{H\odot} \text{ kpc}^{-2} = 16.0 - 0.4 \cdot \mu_e$) and the central velocity dispersion σ_0 . This is described by:

$$\log R_e = a \cdot \log \sigma_0 + b \cdot \log I_e + c \quad (2)$$

Many methods are available for inferring the values of a , b , c . We have considered the *Orthogonal Error Weighted* (OEW) and the *Measurements errors and Intrinsic Scatter* (MIST, see La Barbera et al. 2000) fitting procedures. The OEW method (developed by M. Scodégio, S. Zibetti and P. Franzetti) is based on the minimisation of the error-weighted distance of the measured points from the plane. Details on the mathematical treatment and a full description of the method are given in Appendix A. The MIST method requires an “a priori” determination of the covariance matrix for error and intrinsic scatter. The first one has been estimated as the mean error covariance matrix for the sample. Lacking any reliable model for the intrinsic scatter, the correspondent covariance matrix has been defined null. We consider the results for a number of different fitting procedures and parameters, and separately for the whole dynamical sample (135 galaxies) and for the subsample of 120 galaxies having

$(\sigma_0 > 100 \text{ km sec}^{-1})$ ³: they are presented in Table 2 and in the panels A) and B) of Fig.2. The columns in Table 2 are as follows:

- (1) fitting method: MIST or OEW;
- (2) type of MIST fit: bisector (BIS) or using $\text{Log}R_e$ as dependent variable (Y3);
- (3) error correlation for $\text{Log} I_e$ - $\text{Log} R_e$: if *yes* $\sigma_{\text{Log} R_e \text{ Log} I_e}^2 \sim 0.015 \sim 1.2 \sigma_{\text{Log} R_e} \cdot \sigma_{\text{Log} I_e}$ is assumed; if *no* errors on $\text{Log} I_e$ and $\text{Log} R_e$ are considered uncorrelated⁴;
- (4) lower limit on σ_0 (km sec^{-1});
- (5)-(6) a and associated $1-\sigma$ (68.3% confidence level) error;
- (7)-(8) b and associated $1-\sigma$ (68.3% confidence level) error.

³Values of $\sigma_0 < 100 \text{ km sec}^{-1}$ are usually affected by noticeable uncertainties.

⁴this is the case if the photometric calibration error is the main source of uncertainty on $\text{Log} I_e$.

Table 2: Fit parameters.

<i>MIST/OEW</i>	<i>type</i>	<i>corr</i>	σ_0	<i>a</i>	<i>err</i>	<i>b</i>	<i>err</i>
(1)	(2)	(3)	(4)	(5)	(6)	(7)	(8)
<i>MIST</i>	<i>BIS</i>	<i>yes</i>	0	1.20	0.11	-0.87	0.04
<i>MIST</i>	<i>Y3</i>	<i>yes</i>	0	1.56	0.13	-1.09	0.08
<i>MIST</i>	<i>BIS</i>	<i>no</i>	0	1.37	0.09	-0.86	0.04
<i>MIST</i>	<i>Y3</i>	<i>no</i>	0	1.42	0.10	-0.89	0.06
<i>MIST</i>	<i>BIS</i>	<i>yes</i>	100	0.56	0.12	-0.95	0.05
<i>MIST</i>	<i>Y3</i>	<i>yes</i>	100	1.47	0.15	-1.19	0.10
<i>MIST</i>	<i>BIS</i>	<i>no</i>	100	1.13	0.12	-0.91	0.04
<i>MIST</i>	<i>Y3</i>	<i>no</i>	100	1.40	0.12	-0.98	0.06
<i>OEW</i>	-	<i>yes</i>	0	1.46	0.1	-0.83	0.07
<i>OEW</i>	-	<i>no</i>	0	1.47	0.1	-0.84	0.07
<i>OEW</i>	-	<i>yes</i>	100	1.38	0.1	-0.88	0.07
<i>OEW</i>	-	<i>no</i>	100	1.41	0.1	-0.87	0.07

Inferred parameters a , b show very large inconsistencies in the case of MIST fit, depending on the sample selection, on the error correlations and on the type of fit, bisector or with an individual dependent variable. On the other hand, OEW fits are more stable and consistent within the error limits. This is illustrated in the panels A) and B) of fig.2.

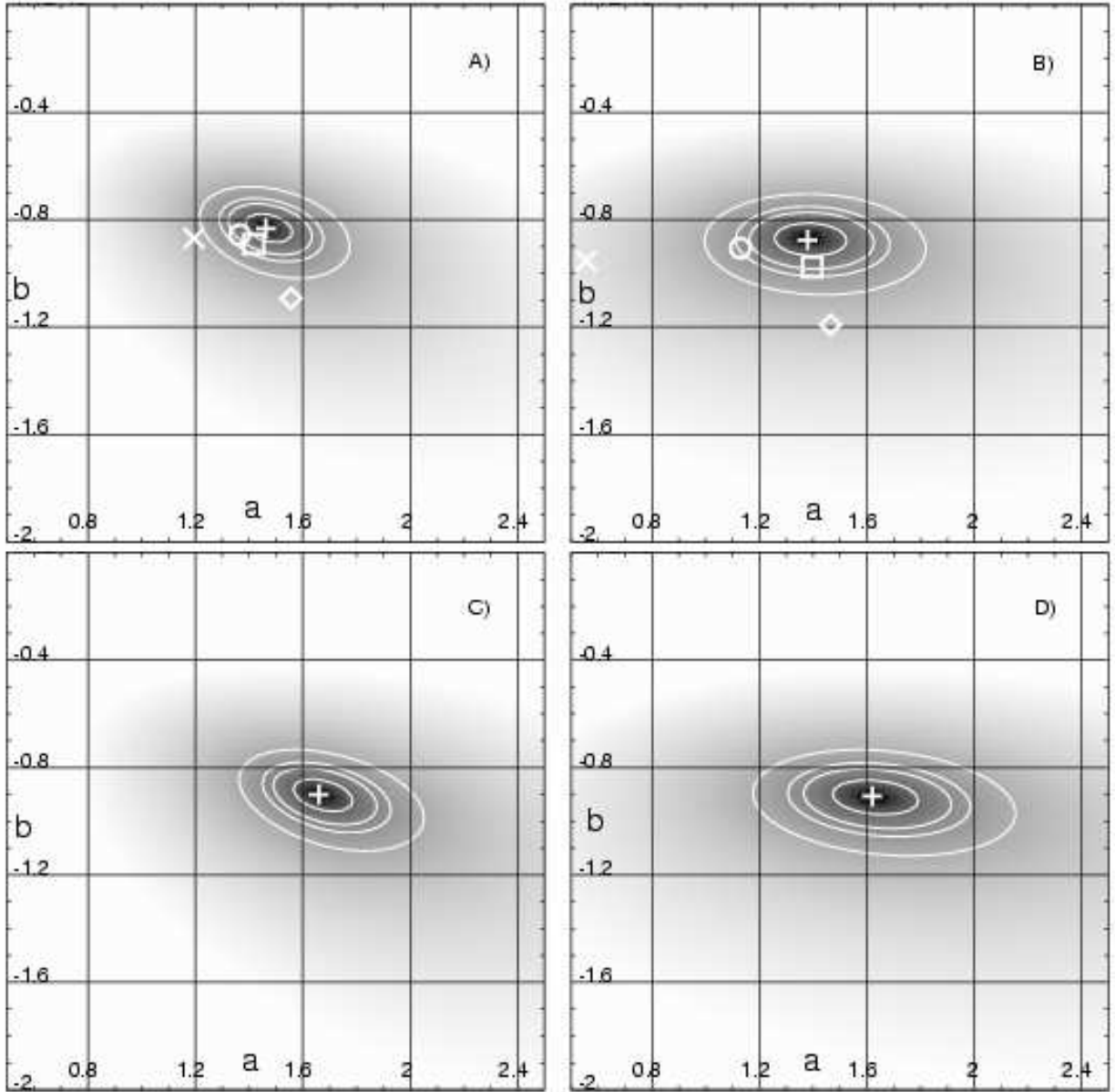


Fig. 2.— The $\Delta\chi^2(a, b)$ distribution with respect to the minimum in logarithmic grey scale for the OEW+correlation fit on the whole sample (A)) and on the sample having $\sigma_0 > 100$ km sec $^{-1}$ (B)). Minimum is marked by a +. Confidence levels of 68.3, 95.4, 99.0 and 99.99% are shown as superposed contour lines. Superposed symbols in panel A) and B) mark best MIST fits for BIS with error correlation (X), Y3 with error correlation (diamond), BIS without correlation (O) and Y3 without correlation (□). Panel C) and D) are the same as A) and B) respectively but using velocity dispersions obtained by the dynamical model (see Sec. 5.1) in the hypothesis of constant $M/L = 1$.

The distribution of the $\Delta\chi^2(a, b)$ with respect to the minimum (marked by a +) is represented in logarithmic grey scale for the OEW+correlation fit on the whole sample (A)) and on the sample having $\sigma_0 > 100 \text{ km sec}^{-1}$ (B)). Confidence levels of 68.3, 95.4, 99.0 and 99.99% are shown as superposed contour lines. Superposed symbols mark best MIST fits for BIS with error correlation (X), Y3 with error correlation (diamond), BIS without correlation (O) and Y3 without correlation (\square). MIST fit results are substantially inconsistent with the OEW results as well, being inside the 95.4% confidence level at best, and outside 99.99% confidence level when error correlation is considered. These inconsistencies are probably due to the high sensitivity of the MIST algorithms to the error and intrinsic scatter model, which is ill-determined.

As our best estimate of the fundamental plane in the H pass-band we adopt the OEW fit with error correlation as applied to the $\sigma_0 > 100 \text{ km sec}^{-1}$ limited sample:

$$\text{Log } R_e = (1.38 \pm 0.1) \cdot \text{Log } \sigma_0 - (0.88 \pm 0.07) \cdot \text{Log } I_e + 5.47 \quad (3)$$

In fig.3 we show the $\text{Log } R_e$ distribution along the fitted plane. The average dispersion is 0.14, which is somewhat higher than the average $1-\sigma$ error associated with $\text{Log } R_e$ (0.09). We conclude that intrinsic scatter is present in the FP relation.

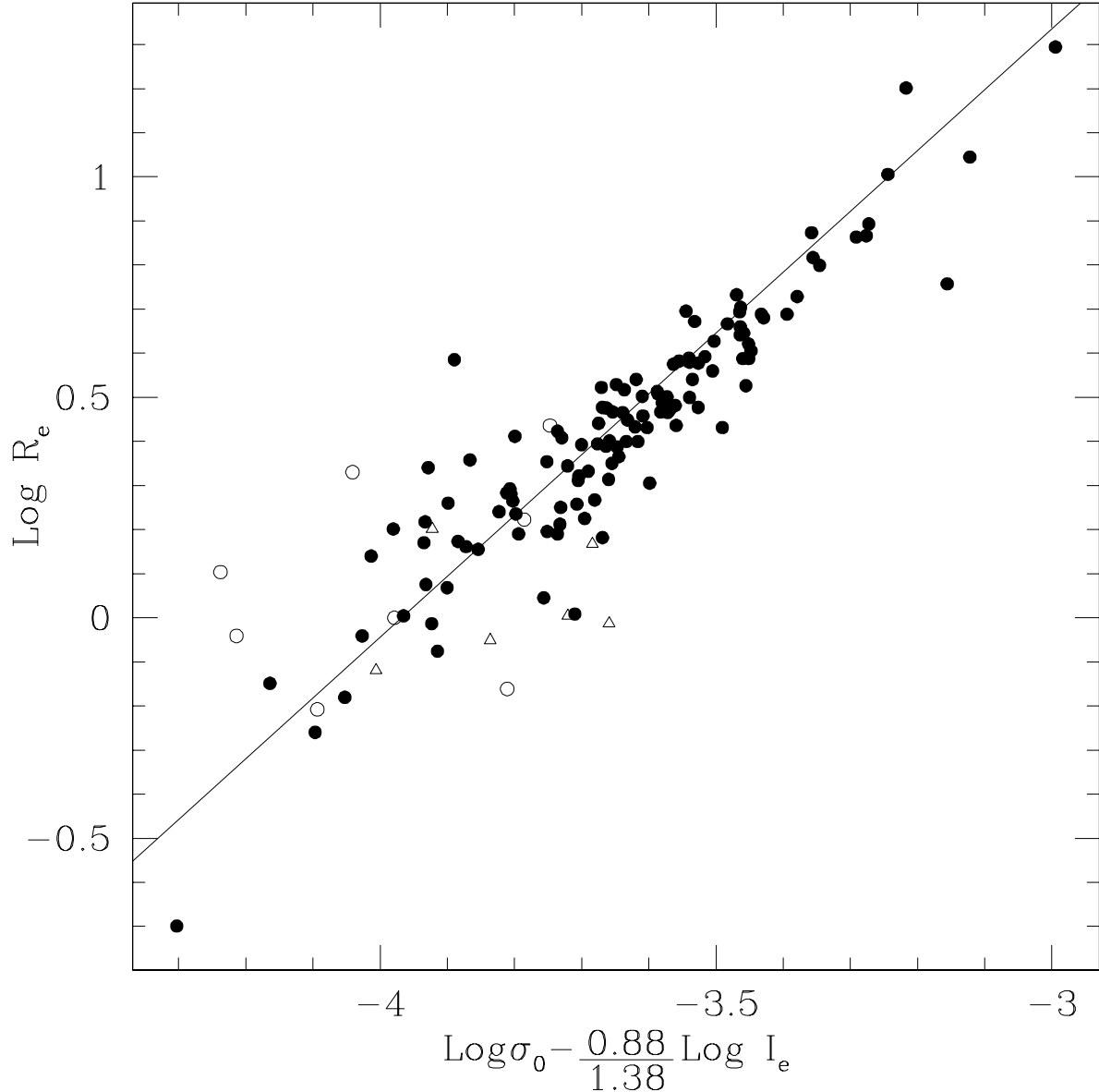


Fig. 3.— A FP section showing $\text{Log } R_e$ distribution along the fitted plane. Triangles identify dwarf galaxies, circles giants. Open symbols are for galaxies having $\sigma_0 < 100 \text{ km sec}^{-1}$. Typical error bars are 0.09 dex along $\text{Log } R_e$ axis and 0.10 dex along the x-axis.

5. Origins of the FP tilt

The zeroth order interpretation of the origins of the FP relationship is derived applying virial equilibrium and the hypothesis that elliptical galaxies form a homological family with respect to their structural and dynamical parameters. That implies:

$$M \cdot \frac{1}{R_g} \propto \langle v^2 \rangle, \quad R_g \equiv \frac{GM^2}{U} \quad (4)$$

$$M \propto \frac{M}{L} \cdot I_e \cdot R_e^2 \quad (5)$$

$$R_g \propto R_e \quad (6)$$

$$\langle v^2 \rangle \propto \sigma_0^2 \quad (7)$$

where M is the total mass, R_g is the gravitational radius, $\langle v^2 \rangle$ is the mean squared velocity of the “particles” (i.e. the stars), G is the gravitational constant and U is the total gravitational potential energy. So the expected equation for the Fundamental Plane is:

$$\log R_e = 2 \cdot \log \sigma_0 - \log I_e - \log \frac{M}{L} + k \quad (8)$$

where the k constant includes all the “shape coefficients” used for translating the observed quantities into the virial ones, as well as the unit conversion factors. According to the homological hypothesis, the difference between the measured coefficients and the expected ones (the so called “tilt” of the FP) is entirely produced by a systematic change in M/L along the galaxy luminosity sequence. This is shown for our sample in fig. 4, using the “ κ space” formalism (Bender et al. 1992) where:

$$\kappa_1 = (\log \sigma_0^2 + \log R_e) / \sqrt{2} \propto \log M \quad (9)$$

$$\kappa_3 = (\log \sigma_0^2 - \log \Sigma_e - \log R_e) / \sqrt{3} \propto \log \frac{M}{L} \quad (10)$$

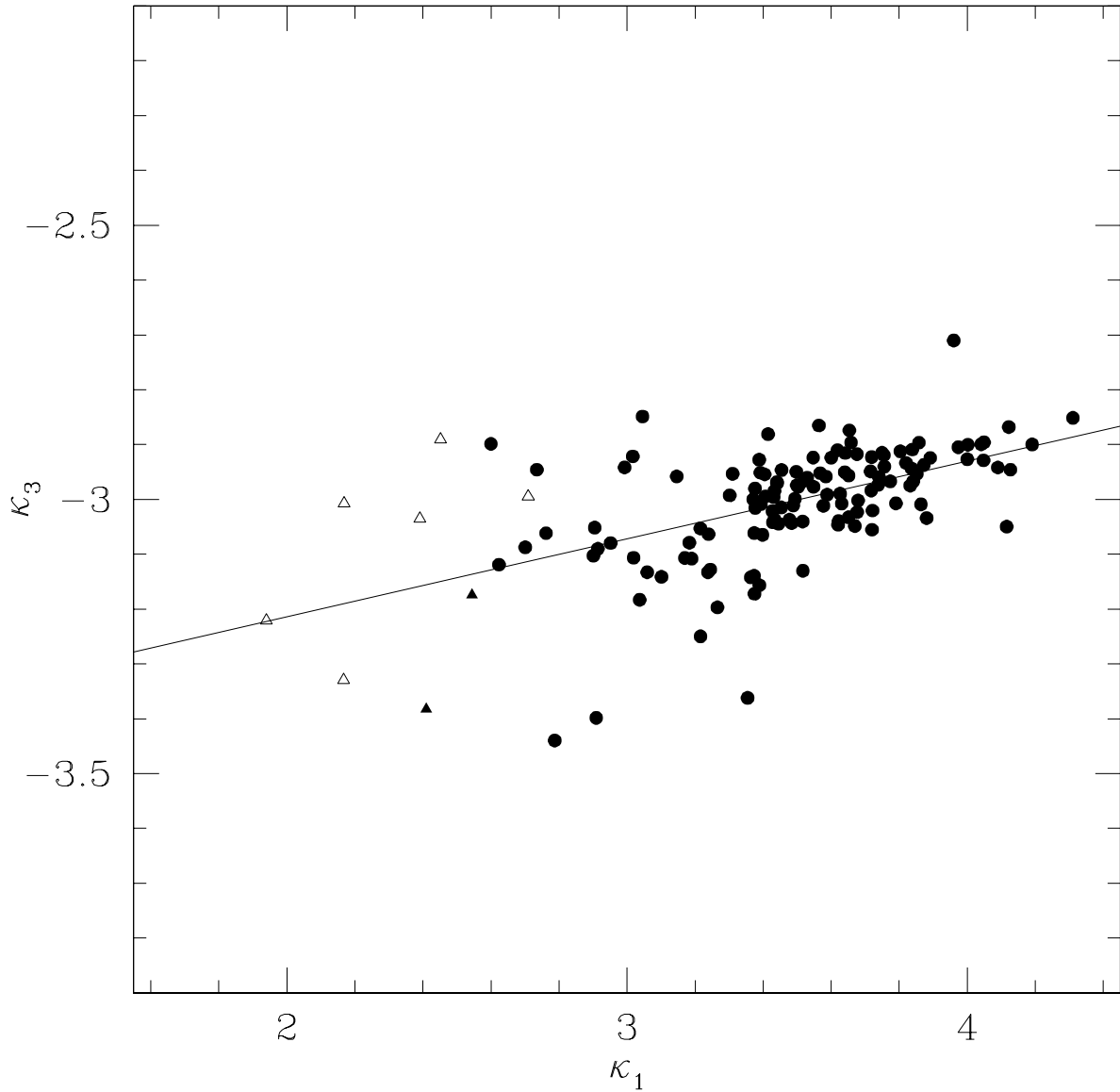


Fig. 4.— The $\kappa_3 - \kappa_1$ projection. Triangles identify dwarf galaxies, circles giants. Open symbols are for galaxies having $\sigma_0 < 100 \text{ km sec}^{-1}$. The continuous line is the best least square fit: $\kappa_3 = 0.14 \cdot \kappa_1 - 3.50$.

A systematic increase in M/L with mass is found, in agreement with the claims of Bender et al. (1992) in B band and Pahre et al. (1998a) in K band.

However, the analysis of surface brightness profiles of elliptical galaxies performed in different pass-bands by many authors during the last years (for the H band see Gavazzi et al. 2001; Scodellgio et al. 2002) demonstrated a systematic change in the profile shapes with luminosity and/or radii, requiring some deviation from pure homology. Systematic variations of the k term in equation (8) have to be taken into account and κ_3 no longer represents a trend of M/L , but results from a combination of M/L and “shape coefficient” effects. In order to disentangle the two contributions we developed the model described in the next section.

5.1. Dynamical model

We model elliptical galaxies as spherically symmetric, isotropic, pressure-supported dynamical systems. Deviations from spherical symmetry and the contribution of rotation to the kinetic energy are neglected (see Ciotti & Lanzoni 1997). M/L is left as a free parameter, but is assumed to be constant within each galaxy. The radial light density profile is derived by de-projection of the measured azimuthally averaged surface brightness profile. This is translated into the mass density profile assuming an initial guess value for $M/L = 1.0$ (solar units). Solving the hydrostatical equilibrium equation the velocity dispersion profile is obtained. The contribution to the Doppler line broadening of each mass element is integrated along the line of sight within a characteristic slit aperture to obtain the model central velocity dispersion $\sigma_{0m} = \sigma_0(M/L)$. M/L is then adjusted to match the measured σ_0 . It is worth noticing here, that the computed values of σ_0 are influenced both by the intrinsic non-homology of the galaxies (i.e. different shapes of mass distribution profiles) and by the aperture effects, due to the different fraction of the galaxy light that contributes to the line broadening inside the slit aperture.

Details on the mathematical treatment are given in appendix B.

5.2. M/L ratios

Unlike in the case of the κ_3 coefficient, the values we derive here for M/L are not influenced by the varying shape of the surface brightness profiles and by the aperture effects.

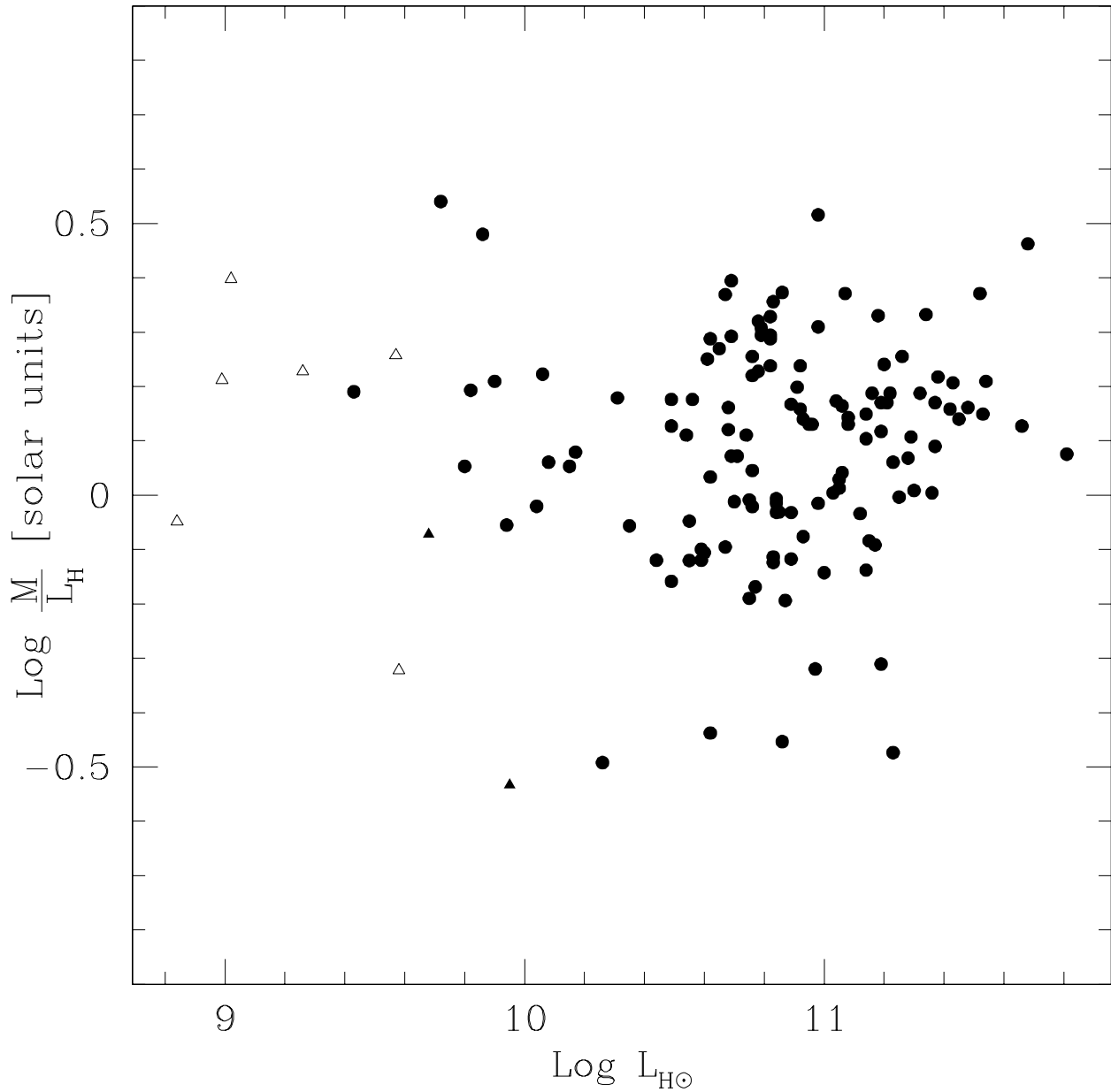


Fig. 5.— The M/L ratios as derived from the model as a function of the total H band luminosity. Symbols as in fig.4.

In fig.5 $\text{Log}M/L$ is shown as a function of the total H band luminosity. No significant evidence of systematic variation of M/L with L can be seen. The average $\text{Log}M/L$ is 0.09 (corresponding to $M/L \sim 1.2$), with a large dispersion of 0.2 *dex*. Systematic variations of M/L are therefore unlikely to be solely responsible for the tilt of the FP. Further evidence comes from replacing the measured values of σ_0 with those obtained from the model assuming a constant M/L for all galaxies⁵: the resulting distribution of the $\Delta\chi^2(a, b)$ is shown in the panels C and D of Fig.2 for the whole dynamical sample and for the subsample with $\sigma_0 > 100 \text{ km sec}^{-1}$ respectively. In both cases the distribution is inconsistent with the values $a = 2, b = -1$ expected on the basis of the virial theorem and homology. This demonstrates that the observed deviations of the profiles from self-similarity are expected to cause a FP tilt similar to that observed, in the absence of any variation in M/L .

5.3. Homology breaking and aperture effects

The dynamical model provides the phase-space density distribution for each galaxy. Potential and kinetic energy can be calculated and the gravitational radius R_g (see equation B7) and the rms velocity $\langle v^2 \rangle^{1/2} \equiv \sigma_{rms}$ can be determined as well. In order to investigate the consequences of the breaking of the homology and of the aperture effects on the coefficients of the FP relation, we study the dependence of the ratios σ_0/σ_{rms} and R_e/R_g on R_e . R_e/R_g does not show any significant correlation with R_e . The relation between σ_0/σ_{rms} and R_e is shown in fig.6.

⁵The exact value of M/L is irrelevant in order to obtain the a and b coefficients. $M/L = 1.0$ has been assumed for simplicity.

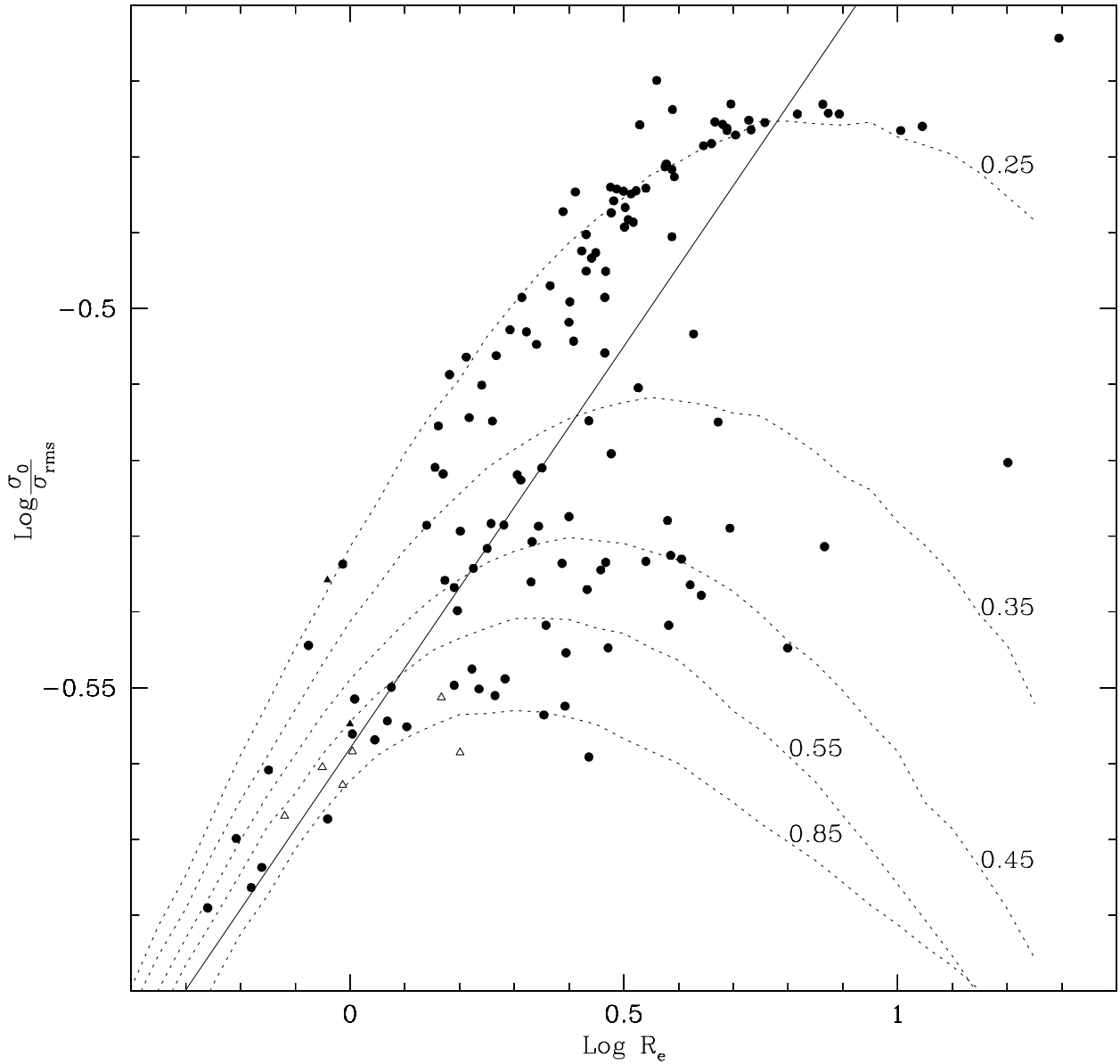


Fig. 6.— The σ_0/σ_{rms} ratio as a function of R_e . Symbols as in fig.4. The continuous line represents the Orthogonal Least Squares Bivariate fit. The dashed lines represent the theoretically expected relation for families of homologous galaxies modelled by Sérsic laws: each curve is labelled with the corresponding ν index.

The clear correlation observed between these two parameters demonstrates that the commonly assumed linear proportionality between σ_0 and σ_{rms} (eqtn.7) does not hold. In principle, this can be a consequence both of an aperture effect, depending on the slit aperture relative to R_e , and of the different velocity dispersion profiles.

The Orthogonal Least Squares Bivariate fit for the points gives

$$\text{Log} \frac{\sigma_0}{\sigma_{rms}} = 0.106 \cdot \text{Log} R_e - 0.558 \quad (11)$$

and is shown as the solid line. The dashed lines superposed to fig.6 show the theoretically expected aperture effect for homologous galaxies following the Sérsic's law⁶ (Sersic 1968) with index $\nu = 0.25, 0.35, 0.45, 0.55, 0.85$. Each curve reflects the dependence of the velocity dispersion on the radius and presents a linearly increasing part, whose slope is largely independent from ν , followed by a maximum and a decreasing part, whose location and slope strongly depend on ν . It is evident that the slope of the mean relation is largely determined by the aperture effect in its linear part, while the non-homology of the light profiles (given by the different ν index) mostly contributes to the scatter. Inserting the average relation in the virial FP equation (8), the FP coefficients $a = 1.65$ and $b = 0.83$ are obtained. Such values are in very good agreement (within 68.3% confidence level) with those obtained fitting the FP on the data sample in which σ_0 was replaced by the central velocity dispersion modelled assuming constant M/L (see fig.2 panels C), D)). The agreement with the “real” FP coefficients is worse, though within the 99.99% confidence level (see Fig.2 panels A), B)).

6. Discussion

The analysis performed in Sec.4 confirms the existence of the FP relation in the NIR H-band claimed by Scodeggio et al. (1998). The inconsistencies between the plane coefficients obtained applying different fitting techniques stresses the fact that comparison between different FP determinations has to be done using homogeneous fitting methods and, in any case, using large samples of galaxies. Due to its stability, irrespective of different hypotheses on the covariance matrix, the OEW fit appears to be the most reliable one. Our determination of FP in H pass-band ($a = 1.38 \pm 0.1$, $b = -0.88 \pm 0.07$, $c = 5.47$, see fig.2) is consistent within $1-\sigma$ with that obtained by Scodeggio et al. (1998) using a subsample of 73 of our galaxies in the Coma cluster and with that obtained by Pahre et al. (1998a) in

⁶ $I(r) = I_0 \text{Exp}(-(r/a)^\nu)$, where I_0 is the central surface brightness, ν is the index ($\nu = 0.25$ corresponding to a deVaucouleurs profile, $\nu = 1$ to an exponential), and a is the scale factor.

K band with a slightly different fitting method. In our analysis we did not apply any correction for the sample incompleteness bias. The method used to calculate such corrections (see Scodeggio et al. 1998, and references therein) relies on Monte Carlo simulations to generate a synthetic sample of galaxies reproducing the observed relations between the galaxy luminosity and the observable quantities involved in the FP. However, such relations are very poorly determined when extended to the faint objects and this affects severely the reliability of the bias corrections. Moreover, although the present sample represents a significant extension of the one considered by Scodeggio et al. (1998) toward low luminosities, we find that the values of the FP coefficients determined in the present work are closer to the uncorrected ($a = 1.51 \pm 0.09$, $b = -0.80 \pm 0.03$) than to the corrected ($a = 1.66 \pm 0.10$, $b = -0.85 \pm 0.03$) ones in Scodeggio et al. (1998), thus indicating that the assumptions underlying the bias correction may be incorrect.

Applying a dynamical model to the measured surface brightness profiles the resulting FP tilt and its origins have been studied. This model represents a higher order approximation than that given by the homological hypothesis, as the “shape coefficients” translating the measured parameters into the virial ones are allowed to vary according to the observed surface brightness profile. Only two assumptions on the structure and dynamics are made:

- M/L is constrained to be homogeneous within each galaxy;
- spherical symmetry and isotropic velocity dispersion are assumed.

Real galaxies are actually much more complex systems; nevertheless it is worth noticing that discrepancies from this description are not likely to affect our conclusions considerably. The use of NIR pass-band photometry minimises the variation of M/L due to different stellar populations. Moreover Ciotti & Lanzoni (1997) showed that asymmetry and anisotropy affect only slightly the kinetic energy in elliptical galaxies modelled according to Sérsic profiles. Contrary to results of Pahre et al. (1998a) in K band and by several authors in optical passbands (see e.g. Bender et al. 1992), the M/L ratio estimated on the basis of our dynamical model in H band does not show any significant increase with luminosity. The H band luminosity appears to be a good first-order estimator for the dynamical mass of elliptical galaxies, in analogy to the claim by Gavazzi et al. (1996), who found direct proportionality between the H-band luminosity and dynamical mass for disk systems.

In turn, the constancy of M/L implies that the tilt of the FP ($\sim 56^\circ$) is mainly caused by a systematic variation in the laws that translate the observed parameters into the virial ones. In fact, we found that the ratio R_e/R_g does not present any systematic variation (spatial homology holds), while the ratio σ_0/σ_{rms} increases with increasing R_e . As demonstrated in Sect.5.3, this is mainly consequence of the “aperture effects”, that strictly related to the

way σ_0 is measured, rather than of structural non-homology. The systematic variation of σ_0/σ_{rms} can entirely account for the tilt of the synthetic FP ($\sim 53^\circ$) in which σ_0 has been computed from the model assuming constant M/L . Moreover this leads to the conclusion that the kinetic energy scales approximately as $\sigma_0^{1.65}$ instead of σ_0^2 , in agreement with the claim of Busarello et al. (1997). However, some residual systematic variation of M/L and R_e/R_g is required to account for the tilt of the measured FP.

The analysis performed by Bertin et al. (2002) by applying a similar dynamical model on a sample of 14 galaxies observed in B-band, concluded that, though no strict homology holds for the elliptical galaxies, a non-negligible contribution from M/L variation is needed to account for the tilt of the FP in B-band. However, no aperture effects are considered in this work, and this in turn could lead to overestimate the contribution due to the M/L variation. The tilt has been proved to increase at shorter wavelengths (see Scodéggi et al. 1998; Pahre et al. 1998a). In principle this could be due either to systematic variations of the global M/L ratio at the shorter optical wavelengths or to the different way in which the aperture effects and non-homology act with respect to the NIR pass-bands, e.g. due to colour gradients. However, Scodéggi et al. (2002) showed that the colour-magnitude relation $B - H$ vs. H for the ellipticals is very flat. Given the constancy of M/L in H-band, this in turn rules out large variations of global M/L as a main cause of the increased tilt of FP at shorter wavelengths. The influence of the aperture effects and of the profile shapes on the tilt in the optical B and V bands will be analysed in a forthcoming paper.

The tightness of the FP relation shows that the causes of the tilt, whatever they are, should act while preserving a structural and dynamical continuity along the sequence of ellipticals. The structural continuity between the giant and the dwarf regime is confirmed also by the Kormendy projection of the FP (see Sec.3). An important point emerging from the $R_e - \mu_e$ distribution is the existence of a cut-off in the effective surface brightness: the upper limit in surface brightness decreases with increasing effective radius, with the same slope of the Kormendy relation for giants.

7. Summary and conclusions

We have determined the Fundamental Plane of elliptical galaxies in nearby rich clusters (mainly Virgo and Coma) in NIR H pass-band. Our result may be written: $\log R_e = (1.38 \pm 0.1) \log \sigma_0 - (0.88 \pm 0.07) \log I_e + 5.47$

The relation is tight, showing a dispersion of 0.14 dex in R_e , while typical errors are 0.09 dex . The origins of the tilt of the fitted plane with respect to the virial predictions for a homologous family of galaxies have been investigated by means of a simple dynamical model. Spherical symmetry, hydrodynamical equilibrium and isotropic velocity dispersion are as-

sumed. Constant M/L within each galaxy has been assumed as a free parameter and used to calculate density and velocity dispersion profiles. M/L was then adjusted in order to match predicted values of σ_0 with the measured ones.

The obtained values of M/L do not show any dependence on the total luminosity. Systematic variations of M/L are then ruled out as the main cause of the tilt of the Fundamental Plane. We showed the ratio between the rms velocity and the central velocity dispersion is systematically varying as a function of R_e , mainly due to the different slit aperture relative to R_e in the spectroscopic measurement of σ_0 . This variation is responsible for most of the amount of the tilt.

The constancy of M/L makes the H-band total luminosity a reliable and cheap first-order estimator for the dynamical mass of elliptical galaxies. This matches the analogous claim by Gavazzi et al. (1996) for disk galaxies.

Applying the dynamical model to datasets extended to low-luminosity and dwarf elliptical galaxies, that will become available in the future, will provide crucial informations in order to determine whether the hypotheses of constant M/L and pure isotropic pressure support can describe (at least in first approximation) the whole family of ellipticals. The structural continuity between the giant- and the dwarf- regime is shown by the distribution of galaxies in the μ_e - R_e plane. The existence of an upper-limit to the effective surface brightness has been found which follows the classical Kormendy relation for the giants.

We thank Gianni Busarello and Francesco La Barbera for kindly providing the MIST code and for helpful advice, and Simon D. M. White for the useful discussion.

A. OEW fit

The Orthogonal Error Weighted fit minimises the orthogonal χ^2 , defined by the sum of the squared distances from the fitted plane, weighted on the errors. This writes:

$$\chi^2 = \sum_i \frac{d^2(i)}{\delta_d^2} \quad (\text{A1})$$

where distances are defined by

$$d(i) = \sqrt{\frac{(a \log \sigma_0(i) + b \log I_e(i) + c - \log R_e(i))^2}{1 + a^2 + b^2}} \quad (\text{A2})$$

and corresponding errors are

$$\delta_d = \sqrt{\frac{a^2 \delta_{\sigma_0}^2 + b^2 \delta_{I_e}^2 + \delta_{R_e}^2 - 2 b \delta_{I_e} \delta_{R_e} r}{1 + a^2 + b^2}} \quad (A3)$$

In the last equation δ_{σ_0} , δ_{I_e} , δ_{R_e} are the errors on the logarithm of the corresponding quantities, r is the error correlation factor between $\text{Log}I_e$ and $\text{Log}R_e$ (see Sec. 3). The minimum is approached using a Powell algorithm (see Press et al. (1992)) starting from an initial guess value in the 3-space of the FP coefficients obtained combining the linear fits on the three projections of the plane.

B. The dynamical model

The dynamical model adopted in this paper for the elliptical galaxies assumes:

- spherical symmetry;
- isotropic velocity dispersion tensor;
- hydrostatic equilibrium;
- homogeneous M/L ratio throughout the galaxy.

The light density distribution $\nu(r)$ is obtained de-projecting the azimuthally averaged surface brightness profile via the inversion of the Abel integral (Binney & Tremaine (1987), eqtn. 4.58a):

$$\nu(r) = -\frac{1}{\pi} \int_r^\infty \frac{dI(R)}{dR} \frac{dR}{\sqrt{R^2 - r^2}} \quad (B1)$$

Due to the inconsistencies (negative light density) induced by irregularities and slope inversions in the empirical profiles, these are replaced in the calculations by the profiles fitted according to analytical laws: deVaucouleurs ($r^{1/4}$, de Vaucouleurs (1948)), exponential, bi-component (exponential+exponential or exponential+deVaucouleurs) and exponentially truncated deVaucouleurs or exponential (see Gavazzi et al. (2000a) and Gavazzi et al. (2001) for details).

Assuming an initial guess value for the M/L ratio, the mass density profile is obtained:

$$\rho(r) = \frac{M}{L} \cdot \nu(r) \quad (B2)$$

For isotropic dispersion tensor the equation for the hydrostatic equilibrium may be written:

$$\frac{d}{dr} [\sigma_r^2(r)\rho(r)] = -\frac{GM(r)\rho(r)}{r^2} \quad (\text{B3})$$

By solving the latter, we obtain the radial velocity dispersion profile:

$$\sigma_r^2(r) = \frac{G}{\nu(r)} \frac{M}{L} \int_r^\infty \frac{L(r')\nu(r')dr'}{r'^2} \quad (\text{B4})$$

Typical dispersion profiles show a maximum which is more peaked and nearer the centre the more cuspy the density profile is, in agreement with the claims by Binney (1980) and of Ciotti & Lanzoni (1997) for the deVaucouleurs and different Sérsic profiles.

Integrating the light weighted contributions to the Doppler line broadening inside a standard slit aperture (corresponding to 2 arcsec by 6 arcsec at the distance of Coma) the expected central velocity dispersion σ_{0m} is obtained. As σ_{0m} goes as $(M/L)^{1/2}$, M/L is consequently adjusted in order to obtain $\sigma_{0m} = \sigma_0$ for the galaxies in the dynamical sample. For the other galaxies an average $M/L \sim 1.2$ is assumed.

Given the hypotheses above and the density and velocity dispersion profiles, the phase space distribution function $f(\vec{r}, \vec{v})$ is completely determined and can be used to obtain the total gravitational potential energy

$$U = -4\pi \int_0^\infty r^2 dr \frac{G M(r)\rho(r)}{r} \quad (\text{B5})$$

and the total kinetic energy

$$K = \int \int \left(\frac{1}{2} |\vec{v}|^2 \right) \cdot f(\vec{r}, \vec{v}) d^3\vec{r} d^3\vec{v} \quad (\text{B6})$$

In turn, this yields:

$$R_g = \frac{GM^2}{U} \quad (\text{B7})$$

$$\sigma_{rms} \equiv \langle v^2 \rangle^{1/2} = \sqrt{2K/M} \quad (\text{B8})$$

All calculations are implemented numerically in a C code written by S.Z. relying on standard algorithms taken from Press et al. (1992). High numerical accuracy is obtained: the $K/|U|$ ratio differs from the expected virial value of 1/2 by less than 10^{-4} at most.

REFERENCES

Bender, R., Burstein, D., & Faber, S. M. 1992, *ApJ*, 399, 462

Bertin, G., Ciotti, L., & Del Principe, M. 2002, *A&A* in press

Binggeli, B., Sandage, A., & Tammann, G. A. 1985, *AJ*, 90, 1681

Binney, J. 1980, *MNRAS*, 190, 873

Binney, J. & Tremaine, S. 1987, *Galactic dynamics* (Princeton, NJ, Princeton University Press, 1987, 747 p.)

Busarello, G., Capaccioli, M., Capozziello, S., Longo, G., & Puddu, E. 1997, *A&A*, 320, 415

Capaccioli, M., Piotto, G., & Rampazzo, R. 1988, *AJ*, 96, 487

Ciotti, L. & Lanzoni, B. 1997, *A&A*, 321, 724

de Carvalho, R. R. & da Costa, L. N. 1988, *ApJS*, 68, 173

de Vaucouleurs, G. 1948, *Annales d'Astrophysique*, 11, 247+

Djorgovski, S. & Davis, M. 1987, *ApJ*, 313, 59

Djorgovski, S., Davis, M., & Kent, S. 1985a, in *New Aspects of Galaxy Photometry*, 257–261

Djorgovski, S., Davis, M., & Kent, S. 1985b, in *New Aspects of Galaxy Photometry*, 257–261

Dressler, A., Lynden-Bell, D., Burstein, D., et al. 1987, *ApJ*, 313, 42

Faber, S. M. & Jackson, R. E. 1976, *ApJ*, 204, 668

Gavazzi, G., Boselli, A., Scodéglio, M., Pierini, D., & Belsole, E. 1999, *MNRAS*, 304, 595

Gavazzi, G., Franzetti, P., Scodéglio, M., Boselli, A., & Pierini, D. 2000a, *A&A*, 361, 863

Gavazzi, G., Franzetti, P., Scodéglio, M., et al. 2000b, *A&AS*, 142, 65

Gavazzi, G., Pierini, D., & Boselli, A. 1996, *A&A*, 312, 397

Gavazzi, G., Zibetti, S., Boselli, A., et al. 2001, *A&A*, 372, 29

Graham, A. & Colless, M. 1997, *MNRAS*, 287, 221

Jedrzejewski, R. I. 1987, *MNRAS*, 226, 747

Kormendy, J. 1985, *ApJ*, 295, 73

Kormendy, J. & Djorgovski, S. 1989, *ARA&A*, 27, 235

La Barbera, F., Busarello, G., & Capaccioli, M. 2000, *A&A*, 362, 851

Pahre, M. A., de Carvalho, R. R., & Djorgovski, S. G. 1998a, *AJ*, 116, 1606

Pahre, M. A., Djorgovski, S. G., & de Carvalho, R. R. 1998b, *AJ*, 116, 1591

Pierini, D., Gavazzi, G., Franzetti, P., Scodéglio, M., & Boselli, A. 2002, *MNRAS* in press

Press, W. H., Teukolsky, S. A., Vetterling, W. T., & Flannery, B. P. 1992, Numerical recipes in C. The art of scientific computing (Cambridge: University Press, —c1992, 2nd ed.)

Prugniel, P. & Simien, F. 1997, *A&A*, 321, 111

Schombert, J. M. 1986, *ApJS*, 60, 603

—. 1987, *ApJS*, 64, 643

Scodéglio, M., Gavazzi, G., Belsole, E., Pierini, D., & Boselli, A. 1998, *MNRAS*, 301, 1001

Scodéglio, M., Gavazzi, G., Franzetti, P., et al. 2002, *A&A*, 384, 812

Sersic, J. L. 1968, in *Atlas de Galaxies Australes*; Vol. Book; Page 1, 0000+

Zibetti, S. 2001, Studio di galassie ellittiche nane d’ammasso nel vicino infrarosso (Tesi di Laurea, Università degli Studi, Milano)

Zwicky, F., Herzog, E., & Wild, P. 1968, Catalogue of galaxies and of clusters of galaxies (Pasadena: California Institute of Technology (CIT), 1961-1968)